Hindawi Publishing Corporation
Shock and Vibration
Volume 2016, Article ID 6239281, 11 pages
http://dx.doi.org/10.1155/2016/6239281

Research Article

Dynamic Characteristics and Experimental Research of Dual-Rotor System with Rub-Impact Fault

Hongzhi Xu, Nanfei Wang, Dongxiang Jiang, Te Han, and Dewang Li

State Key Laboratory of Control and Simulation of Power System and Generation Equipment, Department of Thermal Engineering, Tsinghua University, Beijing 100084, China

Correspondence should be addressed to Nanfei Wang; wnf14@mails.tsinghua.edu.cn

Received 13 June 2016; Accepted 1 August 2016

Academic Editor: Nuno M. Maia

Copyright © 2016 Hongzhi Xu et al. This is an open access article distributed under the Creative Commons Attribution License, which permits unrestricted use, distribution, and reproduction in any medium, provided the original work is properly cited.

Rub-impact fault model for dual-rotor system was further developed, in which rubbing board is regarded as elastic sheet. Sheet elastic deformation, contact penetration, and elastic damping support during rubbing of sheet and wheel disk were considered. Collision force and friction were calculated by utilizing Hertz contact theory and Coulomb model and introducing nonlinear spring damping model and friction coefficient. Then kinetic differential equations of rub-impact under dry rubbing condition were established. Based on one-dimensional finite element model of dual-rotor system, dynamic transient response of overall structure under rub-impact existing between rotor wheel and sheet was obtained. Meanwhile, fault dynamic characteristics and impact of rubbing clearance on rotor vibration were analyzed. The results show that, during the process of rub-impact, the spectrums of rotor vibration are complicated and multiple combined frequency components of inner and outer rotor fundamental frequencies are typical characteristic of rub-impact fault for dual-rotor system. It also can be seen from rotor vibration response that the rubbing rotor's fundamental frequency is modulated by normal rotor double frequency.

1. Introduction

In aero-engine and gas turbine, in order to improve the energy efficiency, reduction of the clearance between the rotor and stator has been widely used. Nevertheless, as the clearance reduces, the physical impact of the rotor on the stationary elements of a rotating machine and the subsequent rubbing at the contact area may happen, which causes complicated vibration that may lead to catastrophic failure. The rotor-to-stator rub-impact results in changes in the system force balance and its dynamic behaviour.

Because of the complexity of the rubbing phenomenon, lots of researches carried out the studies on the rubbing mechanism and dynamic characteristics using numerical simulation or experimental method. Muszynska [1] presented a literature review work on rotor rub related phenomenon and the vibration response in detail, such as impacting, friction, stiffness, and coupling effects. Ahmad [2] reported the rotor-casing contact phenomenon from the perspective of rotor dynamics and described the influences of different system variables such as damping, stiffness, Coulomb friction, and disk flexibility. Beatty [3] proposed a widely accepted mathematical model for rub-impact forces and a detailed response format of diagnostic data in actual cases. Zhang et al. [4] studied dynamic characteristics of micro-rotor system under rub-impact condition with scale-dependent friction model and analysed the effects of control parameters, such as rotating speed, imbalance, damping coefficient, scale length, and fractal dimension. Chen and Zhang [5] presented an overview of the researches on the dynamics of complete aero-engine systems in recent years including the dynamic characteristics analysis of the rubbing of the rotor-casing system. Based on a numerical model and an experimental set-up, Torkhani et al. [6] studied the partial rub of a rotor when rub-impact occurred between the rotor and the nonrotating obstacle under partial light, medium, and severe rub conditions. Abuzaid et al. [7] obtained the vibration responses of a partial rotor-to-stator rubbing by using experimental and analytical methods. Their results demonstrate that vibrations caused by light rubbing are characterized by the integral multiple rotational frequency and serious rubbing by fractional multiple rotational frequency, such as 1/3 and 2/3.

Choi [8] investigated the partial rotor rub experimentally and analytically to understand the rubbing mechanism. Patel et al. [9] proposed a mathematic model composed of rotor and stator and investigated the nonlinear lateral-torsional vibration characteristics of a rotor under rub-impact with a viscoelastically suspended stator. The nonlinear vibration of a rub-impact rotor system was studied by utilizing a special structure of stator, and various periodic and chaotic vibrations were observed in [10].

Because of the complex characteristics of contact phenomena, experimental and empirical methods have been widely used to study the rub-impact mechanism between the stator and rotor. Based on the structural features of turbine casing of aero-engine, the local rub-impact stiffness was simulated in a test rig and vibration characteristics of local rub-impact were analysed by Wang et al. [11]. A general model of a Jeffcott micro-rotor was considered as the research object and the stability of the rub solutions of the rotor system at a high rotating speed were investigated in [12]. The casing was considered as an arc structure with specific angle and the relationship between embedding quantity and normal contact force was established by Ahrens et al. [13]. Chen et al. [14] proposed a novel ball bearing-rotor-stator coupling dynamic model and the dynamic characteristics of rotor and stator under rub-impact condition are analysed. Extensive experiments on a sophisticate "spin-pit" equipment were carried out by Padova et al. [15] and controlled blade-tip/casing interaction and their interpretation are obtained. Wang et al. [16] presented the influences of different physical parameters including rotating speeds, embedding quantities, and casing materials upon the rubbing force when the blade-casing rub-impact occurred. Choy and Padovan [17] discussed the effects of different system variables on contact forces and transient responses of a rub-impact rotor system. The blade-casing rub-impact phenomena were simulated in an underground rotating test-bed in literature [18]. A three-dimensional finite element model was put forward by Bachschmid et al. [19] to simulate the spiral vibration of rub-impact rotor, which were in good accordance with the experiment results. Jacquet-Richardet et al. [20] provided a literature review and checked existing numerical models and experimental equipment utilized for highlighting the phenomena related to different rotor and stator rub-impact configurations.

In this paper, the rub-impact model is proposed to describe the contact force for the impact analysis of the dual-rotor system, in which rubbing board is treated as elastic sheet. In order to describe the characteristics of rub-impact physically, sheet elastic deformation, contact penetration, and elastic damping support during rubbing of sheet and wheel disk are fully considered. Collision force and friction are, respectively, calculated by using Hertz contact theory and Coulomb model, and nonlinear spring damping model and friction coefficient are employed to describe the energy loss during the process of impact. Then kinetic differential equations of rub-impact under dry rubbing condition are derived. Based on one-dimensional finite element model of dual-rotor system, dynamic transient response of overall structure under rub-impact occurring between rotor wheel and sheet is obtained.

Meanwhile, fault dynamic characteristics and the impact of rub-impact clearance on rotor vibration are analysed. The results show that under rub-impact condition, the spectrums of rotor vibration are complicated and multiple combined frequency components of inner and outer rotor fundamental frequencies are typical characteristic of rub-impact fault for dual-rotor system. It also can be seen from rotor vibration response that the rubbing rotor's fundamental frequency is modulated by normal rotor double frequency.

2. Mathematical Model of Rub-Impact Fault for Dual-Rotor System

2.1. Introduction to the Dual-Rotor Experiment Rig. Figure 1 shows the mechanical structure of the considered dual-rotor system. The inner rotor (1) passing though the outer rotor (2) is connected to a flexible coupling that is driven by a high-speed motor; the outer rotor is driven by a high-speed motor with a belt. Every bearing is supported on one pedestal (13), which is fixed on the foundation by several bolts. The bearing pedestal and membrane coupling (12) can reduce the influence of transverse force due to belt driven. The inner rotor and outer rotor are, respectively, installed wheel disks to simulate the compressor and turbine load. Both ends of inner rotor are supported by deep groove ball bearing (4) and roller bearing (5), respectively; one end of outer rotor is supported by deep groove ball bearing (6), and the other end is supported on the inner rotor by means of squirrel cage elastic support and roller bearing (7). Two wheel disks (8, 9) are mounted on the inner rotor, and there are three wheel disks (10, 11, and 12) installed on the outer rotor. The elastic support is installed on the wheel disk, the number of which is (11).

One dimensional finite element model of dual-rotor system (excluding pedestal) is built based on Timoshenko beam element, as presented in Figure 2, which is composed of the inner rotor (node 1 to node 13) with the outer rotor (node 14 to node 20). There are total of four bearings in the model, which are, respectively, located at node 1, node 14, node 9, and node 13, where node 1 and node 13 denote the inter-shaft bearings. The disks, located, respectively, at node 16, node 18, node 3, and node 11, represent the concentrations of high-pressure compressor disks, high-pressure turbine disks, low-pressure compressor disks, and low-pressure turbine disks.

2.2. The Description of Rub-Impact Fault. In aero-engine, the disks installed with multistage blades of compressor and turbine are usually mounted on the rotor system. Aero-engine rotors are supported on stator casing by utilizing ball bearings, and the casing is supported on a base. In generally, the casing is relatively thin. In order to provide the reductions in fuel consumption and improve the structural efficiency, reduction of the tip clearance between the rotating blade and the casing has been widely used. However, as the clearance reduces, the probability of the rubbing occurring under some operational conditions also increases. In the

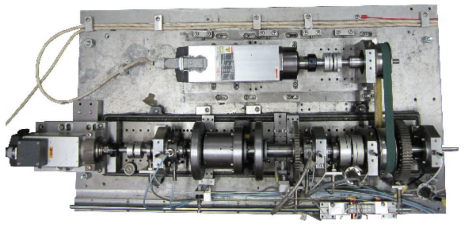

(a) Dual-rotor system test rig

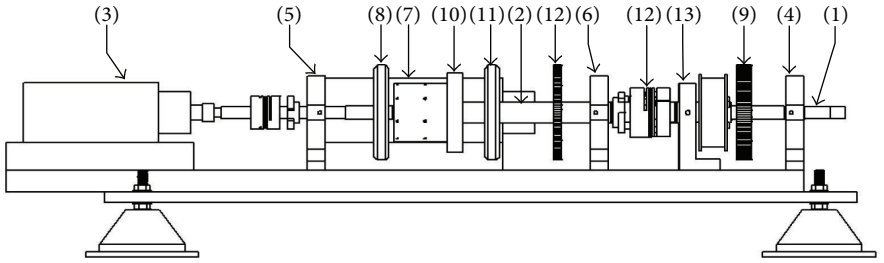

(b) Structure elevation of dual-rotor experiment setup

Figure 1: Dual-rotor system test rig and structure diagram.

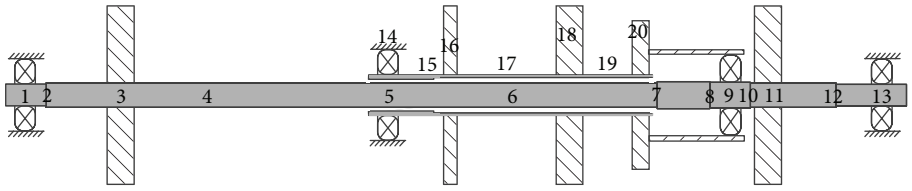

Figure 2: The node map of one dimensional finite element model of dual-rotor system.

initial period of rubbing, the rub-impact occurs between blades and soft coating painted on the casing. With the rubbing fault becoming more serious, the rub-impact existing between blades and casing directly happens, which may cause safety risk and subsequent economic loss.

Based on the rub-impact characteristics, it is assumed that the rub-impact between blades and casing is simplified as point rubbing or local rubbing. For convenience of study, the casing is considered as elastic support plate (hereafter referred to as rubbing plate), and only the rub-impact between disk and rubbing plate is taken into account in the paper, as shown in Figure 3.

When the amplitude of disk is greater than the clearance between the disk and the rubbing plate, the rub-impact will happen. Rubbing fault not only results in the overall vibration of rubbing plate but also causes bending deformation of the plate under elastic support. With the rubbing fault becoming more serious, the contact-penetration phenomenon appears in the local rubbing area. It is supposed that the rub-impact between disk and rubbing plate is considered as dry friction, and the rubbing plate is affected by both normal collision force and tangential friction force. The rub-impact may lead to complicated vibration and deformation of rubbing plate. As for aero-engine, only the acceleration vibration signals can

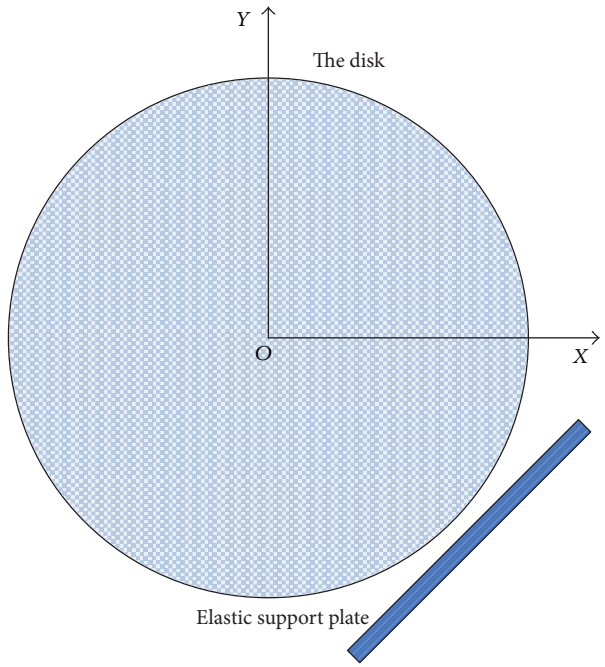

Figure 3: The schematic diagram of rub-impact between rotor disk and plate.

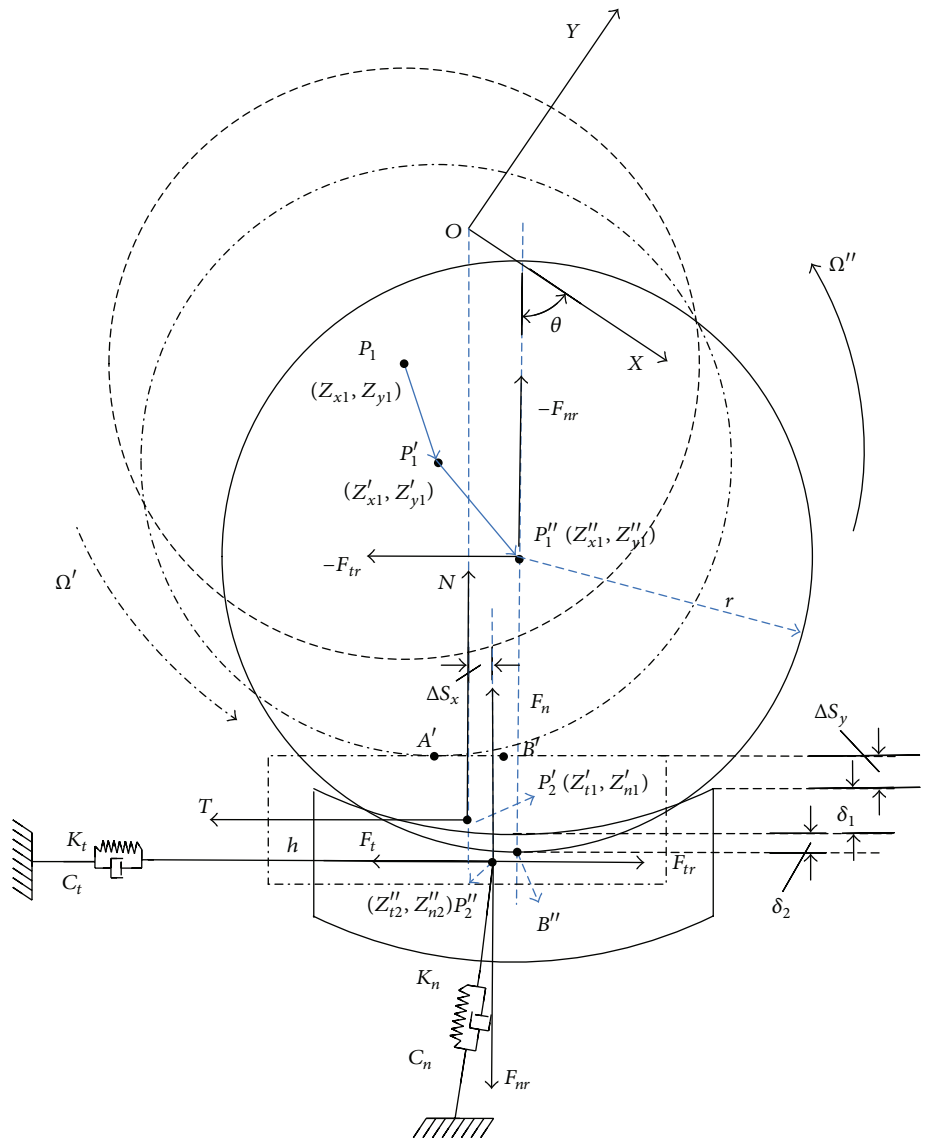

Figure 4: The dynamic model of rub-impact between rotor disk and elastic plate.

be obtained by using the sensors fixed on the casing, and it is relatively to collect the displacement vibration signals of rotors. Because of the complexity of rub-impact phenomenon and strong noise, the acceleration vibration signals picked up from the casing is complicated, which makes it challenging to extract fault features. Hence, in order to study the rub-impact mechanism, it is of significance to build a perfect dynamic model describing the characteristics of rub-impact between disk and rubbing plate.

2.3. The Dynamic Model of Rub-Impact. The deformation of rubbing plate caused by rub-impact between the disk and rubbing plate is supposed to be elastic, and rubbing plate only does motion in normal and tangential directions. Under rub-impact status, the contact between disk and rubbing plate is considered to be tight, and contact, deformation, and penetration exist in the local rubbing area. The overall elastic support of rubbing plate is simplified as normal and tangential linear spring damping support. The dynamic model of rub-impact between disk and rubbing plate is illustrated in Figure 4.

It can be seen from Figure 4 that θ denotes the angle of rubbing plate normal direction and x-axis; P_1, P_1', and P_1'' represent the centre of the disk in different times, namely, before rubbing and rubbing contact moment and in the process of rubbing, respectively; P_2' and P_2'' represent the rubbing plate's centre of gravity in contact moment and in the course of rubbing, respectively. The bending deformation of rubbing plate caused by rub-impact is supposed to be elastic. A' denotes the location where disk contacts with rubbing plate in contact moment; B'' represents the location where disk contacts with rubbing plate at some point in the process of rubbing; ΔS_x and ΔS_y are the motion distance of rubbing plate and also can be seen as spring compression or tension distance in normal and tangential directions at

some point in the course of rubbing, respectively; δ_1 denotes the deflection displacement of contact point when bending deformation of rubbing plate occurs; δ_2 denotes contact deformation displacement occurring between rubbing plate and disk in the local contact area. F_n and F_t stand for normal force and tangential force exerted on the disk by the elastic damping support, respectively; F_{nr} and F_{tr} denote the normal contact pressure and the tangential friction force exerted on the rubbing plate by the disk, respectively. When the relative motion exists between the disk and rubbing plate in tangential direction, F_{tr} is defined as dynamic friction force, otherwise known as static friction force. Correspondingly, $-F_n$ and $-F_t$ are defined as normal force and tangential force exerted on the disk by the rubbing plate.

For convenience of study, two coordinate frames are established. XY coordinate system is set up by using the centre of disk at rest as the origin, as shown in Figure 4. NT coordinate system is built by using the rubbing plate's centre of gravity as the origin, and two axes are defined as the normal and tangential directions of rubbing plate, as shown in Figure 4. The two coordinate systems transformation relations can be expressed as follows:

$$\begin{bmatrix} x' \\ y' \end{bmatrix}_{XY} = \begin{bmatrix} x_0 \\ y_0 \end{bmatrix}_{XY} + \begin{bmatrix} -\sin\theta & -\cos\theta \\ \cos\theta & -\sin\theta \end{bmatrix} \begin{bmatrix} x \\ y \end{bmatrix}_{NT}. \quad (1)$$

$[x_0, y_0]^T$ denotes the rubbing plate's centre of gravity in coordinate frame XY; $[x, y]^T_{NT}$ represents some point in coordinate system NT, and $[x', y']^T_{NT}$ is the corresponding point of $[x, y]^T_{NT}$ in coordinate system XY; θ stands for the angle of rubbing plate's normal direction and x axis. $[x, y]^T_{NT}$ in coordinate system NT corresponding to $[x', y']^T_{NT}$ in coordinate system XY can be written as

$$\begin{bmatrix} x \\ y \end{bmatrix}_{NT} = \begin{bmatrix} -\sin\theta & \cos\theta \\ -\cos\theta & -\sin\theta \end{bmatrix} \begin{bmatrix} x' - x_0 \\ y' - y_0 \end{bmatrix}_{XY}. \quad (2)$$

F'_{nr} denotes the force exerted by the disk, which causes the bending deformation of rubbing plate. Assume that F_{nr} can be further expressed as follows in the course of rub-impact

$$F_{nr} = F'_{nr}. \quad (3)$$

Since the rub-impact area and the bending deformation are relatively small, it is supposed that the bending does not affect the position of the rubbing plate's centre of gravity. Therefore, the overall motion of rubbing plate can be described by motion of its centre of gravity. The normal displacement of the disk consists of three parts, namely, plate's normal displacement, the deflection displacement of bending deformation, and contact deformation of rubbing plate. The displacement relationship can be obtained as

$$\left|P''_1 P'_1\right|_N = \left|B'' B'\right|_N = \Delta S_y + \delta_1 + \delta_2. \quad (4)$$

Here, $|P''_2 P'_2|_N = \Delta S_y$, $|B' P'_1|_N = r$.

Based upon the geometrical relationship, the following expression can be obtained:

$$\begin{aligned} \left|P''_2 P''_1\right|_N &= \left|P''_2 P'_2\right|_N + \left|B' P'_1\right|_N - \left|P''_1 P'_1\right|_N + \frac{h}{2} \\ &= \frac{h}{2} + r - \delta_2 - \delta_1, \end{aligned} \quad (5)$$

where r is the radius of disk and h is the thickness of rubbing plate. In addition, the criteria of rubbing are demonstrated as follows:

$$\begin{aligned} \delta &= \delta_1 + \delta_2 \\ &= \begin{cases} > 0 & \text{No rubbing} \\ = 0 & \text{Rubbing moment} \\ < 0 & \text{Bending and contact deformation of rubbing plate.} \end{cases} \end{aligned} \quad (6)$$

Considering the influences of rub-impact and the external forces on the system vibration, the differential equation of motion of rubbing plate in the coordinate frame NT can be written as follows:

$$\begin{aligned} \mathbf{M}_r \ddot{x}_t + \mathbf{C}_t \dot{x}_t + \mathbf{K}_t x_t &= \mathbf{F}_{tr}, \\ \mathbf{M}_r \ddot{y}_n + \mathbf{C}_n \dot{y}_n + \mathbf{K}_n y_n &= \mathbf{F}_{nr}. \end{aligned} \quad (7)$$

Here, $F_{nr} = H(\delta) \cdot F_{nr} = H(\delta) \cdot (K_{nr} {\delta_2}^{1.5} + c K_{nr} {\delta_2}^{1.5}) = H(\delta) \cdot (c+1) K_{nr} [\delta - W(\xi, \eta)]^{1.5}$:

$$F_{tr} = \begin{cases} -\mu_d \left|F_{nr}\right| \operatorname{sign}(v) & \mu_s \left|F_{nr}\right| > F_{\max} \\ \le \mu_s \left|F_{nr}\right| \operatorname{sign}\left(v'\right) & \mu_s \left|F_{nr}\right| \le F_{\max}. \end{cases} \quad (8)$$

$W(\xi, \eta)$ is the deflection displacement of rubbing plate in the contact point (ξ, η), which can be denoted by δ_1:

$$H(\delta) = \begin{cases} 1, & \delta < 0 \\ 0, & \delta \ge 0. \end{cases} \quad (9)$$

When the edges of rubbing plate are simply supported, the following expression can be obtained by using $F_{nr} = F'_{nr}$:

$$\begin{aligned} (c+1) K_{nr} \left[\delta - w(\xi, \eta)\right]^{1.5} &= W(\xi, \eta) \pi^4 abD \\ &\cdot \left[4 \sum_{m=1}^{\infty} \sum_{n=1}^{\infty} \frac{\sin(m\pi\xi/a) \sin(n\pi\eta/b)}{\left(m^2/a^2 + n^2/b^2\right)^2} \sin\frac{m\pi x}{a} \right. \\ &\left. \cdot \sin\frac{n\pi y}{b} \right]^{-1}. \end{aligned} \quad (10)$$

When one edge of rubbing plate is fixed and other edges are free, the following equation can be acquired:

$$(c+1) K_{nr} \left[\delta - W(\xi, \eta)\right]^{1.5} = a_0 W(\xi, \eta) - b_0. \quad (11)$$

Here, a_0 and b_0 are the fitting coefficients of deflection formula.

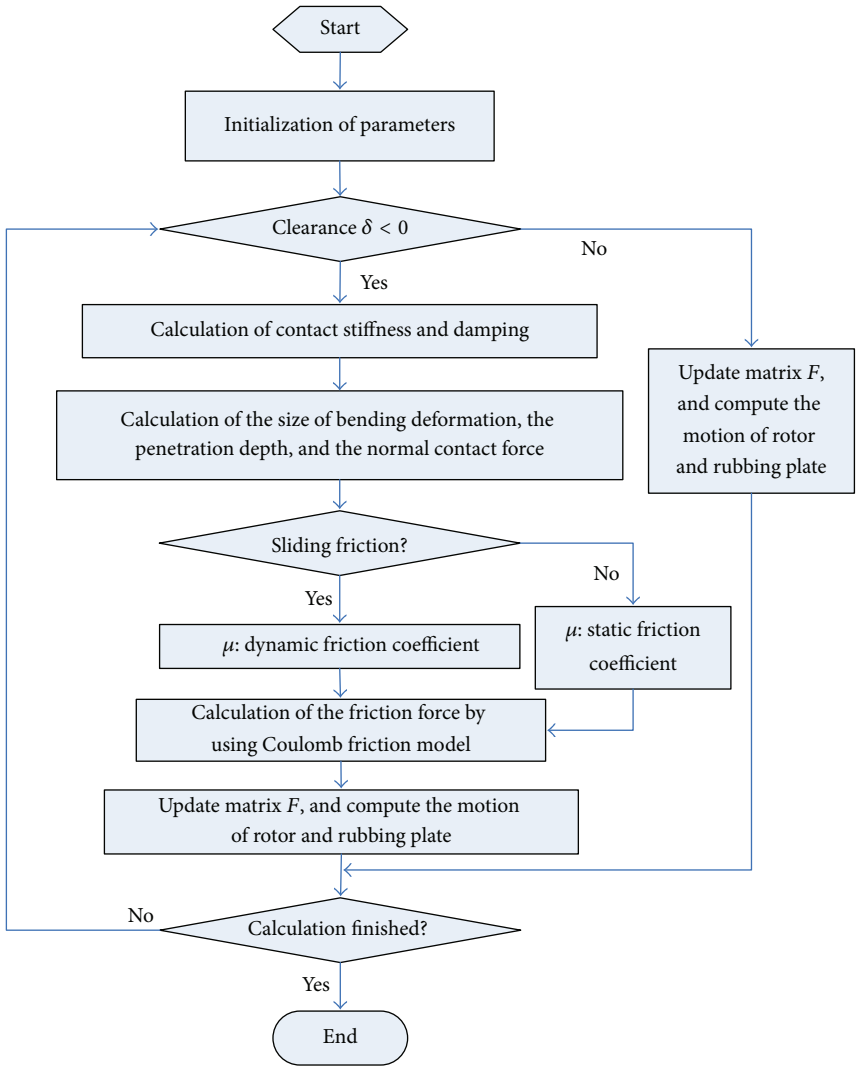

Figure 5: The simulation flow chart of dual-rotor system with rub-impact fault.

Only $W(\xi, \eta)$ is an unknown parameter in (10) and (11), and the solution can be solved by means of nonlinear equations or numerical method.

Under rub-impact status, the force vector exerted on the node of rotor is defined as $\mathbf{F}_L = [F_x, F_y]^T$, where

$$F_x = \begin{cases} F_n \cos\theta + F_t \sin\theta, & \delta < 0 \\ 0, & \delta \geq 0, \end{cases}$$
$$F_y = \begin{cases} F_n \sin\theta - F_t \cos\theta, & \delta < 0 \\ 0, & \delta \geq 0. \end{cases} \quad (12)$$

One dimensional finite element model with four degrees of freedom is utilized in the dual-rotor system, and Newmark-β algorithm is applied to carry out fault simulation. The governing equation of motion described to the overall system can be obtained as follows:

$$(\mathbf{M}_T + \mathbf{M}_R)\ddot{\delta} + (\Omega\mathbf{G} + \mathbf{C})\dot{\delta} + \mathbf{K}_B\delta = \mathbf{F}(t) + \mathbf{F}_L. \quad (13)$$

3. The Simulation Calculation of the Model and Comparison Analysis with Experimental Results

3.1. The Simulation Calculation of Rub-Impact. Considering the elastic deformation, contact-penetration and the motion of rubbing plate, the theoretical model with rub-impact fault of dual-rotor system is derived based on Coulomb friction law and nonlinear contact model. The next step is to solve the governing equations numerically, and the implemented procedure is listed in Figure 5.

The dynamic characteristics of 18th node located in outer rotor under rub-impact status are simulated, and the vibration displacement signals of 14th node are obtained. The rotating speeds of inner rotor and outer rotor are, respectively, set to 4200 rpm (70 Hz) and 5400 rpm (90 Hz) when the simulation calculation is carried out.

The time waveform of inner rotor and outer rotor with rub-impact is shown in Figure 6. It can be observed from

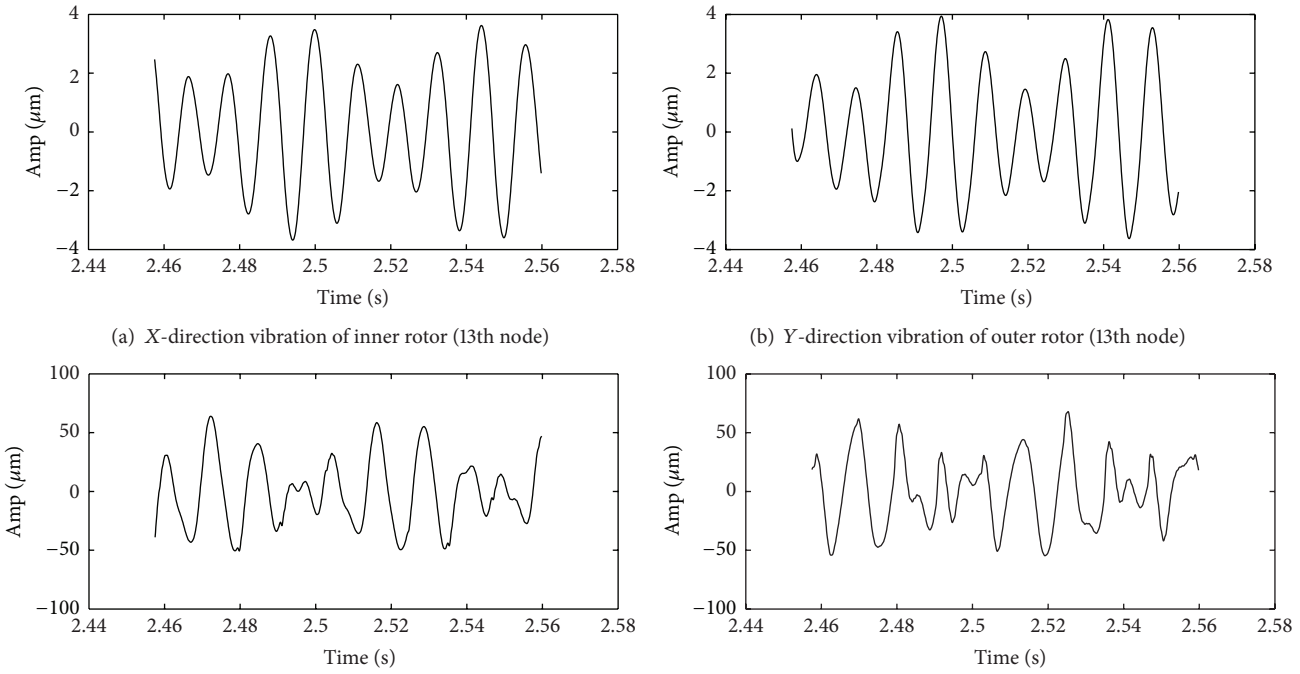

(a) X-direction vibration of inner rotor (13th node)

(b) Y-direction vibration of outer rotor (13th node)

(c) X-direction vibration of inner rotor (14th node)

(d) Y-direction vibration of outer rotor (14th node)

Figure 6: The vibration displacement waveform of inner and outer rotors (rubbing location: outer rotor disc).

Figure 6 that the inner rotor's waveforms in X and Y directions have not significantly changed, but the outer rotor's waveforms in X and Y directions present some characteristics and phenomena, such as waveform cutting and distortion, which may result in complicated spectrum composition.

It should be noted that vibration spectrum only contains fundamental frequencies of inner and outer rotor under normal status, namely, 70 Hz and 90 Hz. In order to extract the rub-impact features, the spectrum of time waveform shown in Figure 6 is presented in Figure 7. It can be seen from Figure 7 that the amplitudes of fundamental frequencies basically remain unchanged, but some frequency components are increased at low and high frequency parts. Especially in high frequency part, the combination frequency and multiple frequency components of fundamental frequencies are obvious. In order to make further observations, the spectrums of inner and outer rotors' waveforms in X- and Y-directions under rub-impact status are demonstrated in Figure 8, respectively.

It can be observed from Figure 8 that the spectrums contain other frequency components in addition to the fundamental frequencies of inner and outer rotors. The additional frequency components and amplitudes are less in spectrums of inner rotor when the rubbing location is set to the outer rotor disk; however, the additional frequency components are more and amplitudes are larger in the spectrums of outer rotor, especially the spectrum in Y-direction. In the next section, the outer rotor spectrum in Y-direction is used as object to analyse the frequency components.

According to a preliminary judgment, other than the fundamental frequencies of inner and outer rotors (69.58 Hz, 90.33 Hz), combined frequencies and super-harmonic frequencies components also have larger amplitudes. Comparing with other frequency components, it can be clearly seen that the sum frequency of inner and outer rotors' fundamental frequencies and $2f_H$ (f_L and f_H represent the fundamental frequencies of inner and outer rotor, resp.) are more obvious. Some special frequency components are listed in Table 1.

From Table 1, besides the fundamental frequencies of inner and outer rotor, sometimes sum frequency and difference frequency and superharmonic frequencies (such as $2f_L$, $2f_H$, $3f_H$, $4f_H$, and $5f_H$) are presented. In addition, the spectrums also contain combined frequencies of fundamental frequencies of inner and outer rotor, namely, $mf_H \pm nf_L$, $(m, n = 1, 2, \ldots)$.

It can be observed from Figure 9 that the axis trajectory of outer rotor shows the disorder characteristics with vortex motion, and the axis trajectory of inner rotor reflects a slight change, which has obvious contraction in rubbing location.

3.2. Experimental Verification. In order to verify the effectiveness of the rub-impact model, rubbing experiments are carried out to simulate the rubbing fault occurring in the outer rotor. The rubbing diagram of dual-rotor system is illustrated in Figure 10. The rubbing disk is located in the outer rotor. The rotating speeds of inner and outer rotors are designed as 4200 rpm (70 Hz) and 5400 rpm (90 Hz), respectively. Fast Fourier Transform (FFT) is performed and spectrums of corresponding model's nodes are obtained, as shown in Figure 11 (black solid line denotes the normal state, and the blue dotted line represents the rubbing fault). Because

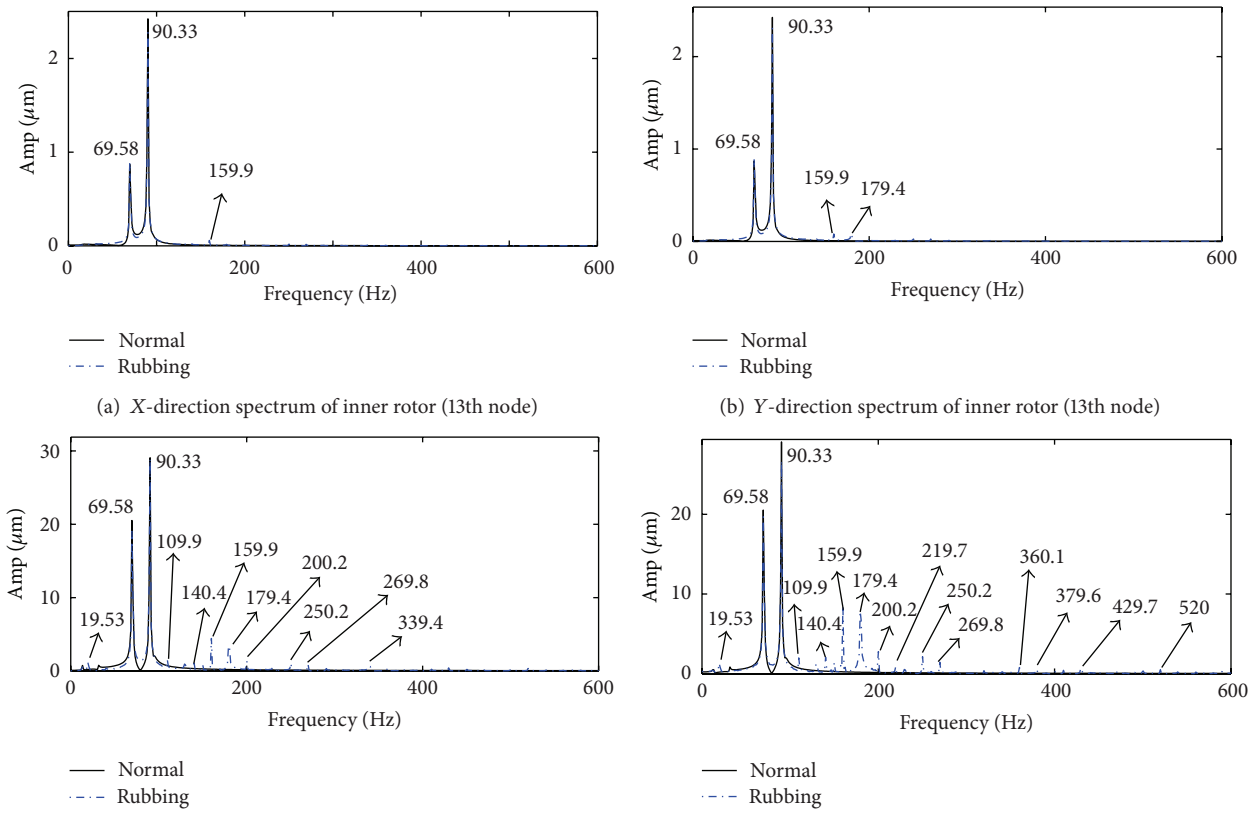

(a) X-direction spectrum of inner rotor (13th node)

(b) Y-direction spectrum of inner rotor (13th node)

(c) X-direction spectrum of outer rotor (14th node)

(d) Y-direction spectrum of outer rotor (14th node)

FIGURE 7: The vibration displacement spectrum of inner and outer rotors (rubbing location: outer rotor disc).

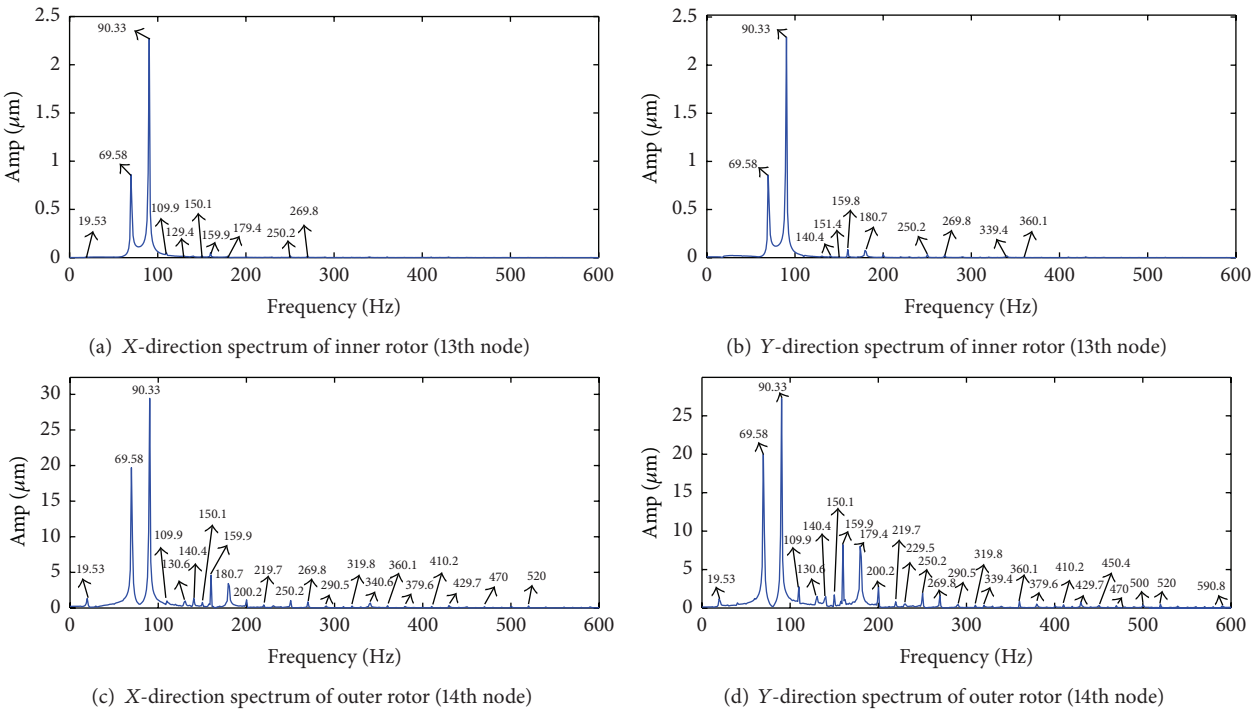

(a) X-direction spectrum of inner rotor (13th node)

(b) Y-direction spectrum of inner rotor (13th node)

(c) X-direction spectrum of outer rotor (14th node)

(d) Y-direction spectrum of outer rotor (14th node)

FIGURE 8: The vibration displacement spectrum of rotors (rubbing location: outer rotor disc).

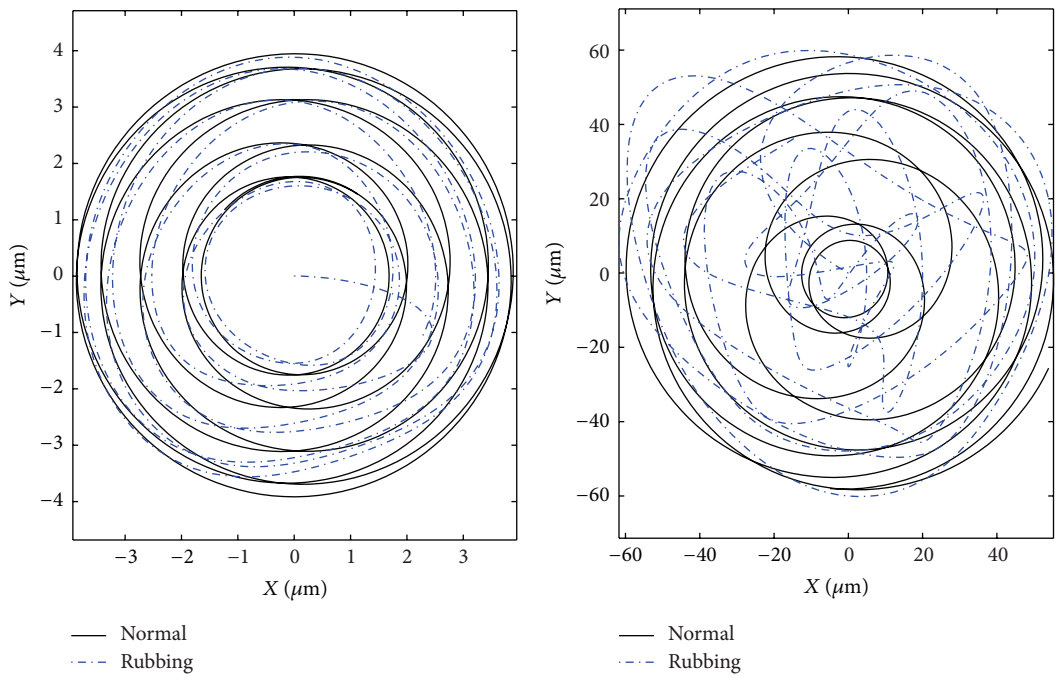

(a) Axis orbit of inner rotor (13th node)

(b) Axis orbit of outer rotor (14th node)

Figure 9: The axis trajectory of rotor (rubbing location: outer rotor disc).

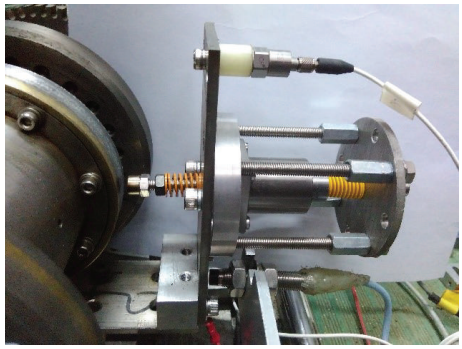

Figure 10: The rubbing diagram of dual-rotor system.

of the small influence of rubbing on the motions of rotors, the ordinate in the spectrum is expressed by using logarithmic in order to facilitate comparison.

Comparing with the normal state, it can be seen from Figure 11 that the spectrums of inner and outer rotors under rubbing condition are more abundant. Meanwhile, the amplitudes in inner rotor's X-direction spectrum are bigger when the frequency components are greater than $3f_L$ (f_L denotes the fundamental frequency of inner rotor, and f_H represents the fundamental frequency of outer rotor). As for the outer rotor, the amplitudes are more prominent when the frequency components are greater than $2f_H$. Since it is difficult to adjust the dual-rotor experimental test rig to the ideal state, there are always some minor faults in the initial period, such as misalignment and pedestal looseness. Under the influence of these factors, the spectrums of inner and outer rotors under normal state also may have many frequency components with small amplitudes. By comparison, the new frequency components or the frequency components with

Table 1: The vibration frequency spectrum component analysis of outer rotor.

Frequency (Hz)	Component
19.53	$f_H - f_L$
109.9	$2f_H - f_L$
130.6	$3f_H - 2f_L$
140.4	$2f_L$
150.1	$4f_H - 3f_L$
159.9	$f_H + f_L$
179.4	$2f_H$
200.2	$3f_H - f_L$
219.7	$4f_H - 2f_L$
230.7	$f_H + 2f_L$
250.2	$2f_H + f_L$
269.2	$3f_H$
290.5	$4f_H - f_L$
319.5	$2f_H + 2f_L$
339.4	$3f_H + f_L$
360.1	$4f_H$
379.6	$5f_H - f_L$
410.2	$3f_H + 2f_L$
429.2	$4f_H + f_L$
450.1	$5f_H$
470	$6f_H - f_L$
500	$4f_H + 2f_L$
520	$5f_H + 2f_L$
590.8	$5f_H + 2f_L$

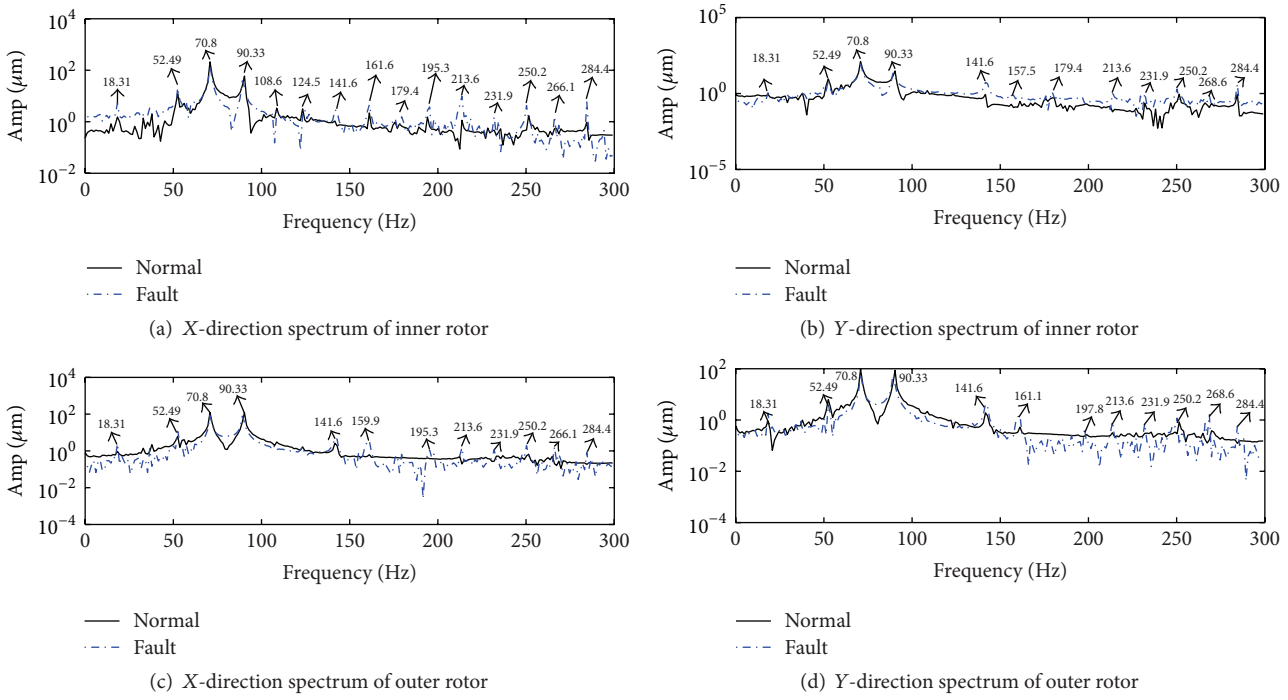

Figure 11: The vibration displacement spectrums of X direction and Y direction.

Table 2: The vibration frequency spectrum component analysis of inner and outer rotor.

Frequency (Hz) (inner rotor)	Component	Frequency (Hz) (outer rotor)	Component
18.31	$f_H - f_L$	18.31	$f_H - f_L$
141.6	$2f_L$	141.6	$2f_L$
195.3	$f_H + 3f_L/2$	159.9	$f_H + f_L$
213.6	$3f_L$	195.3	$f_H + 3f_L/2$
231.6	$f_H + 2f_L$	213.6	$3f_L$
250.2	$2f_H + f_L$	231.6	$f_H + 2f_L$
281.1	$4f_L$	250.2	$2f_H + f_L$
		266.1	$3f_H$
		284.4	$4f_L$

large amplitude change are listed (not including f_L and f_H), as shown in Table 2.

4. Conclusions

In the study, the rubbing fault is simulated by using dynamic model and dual-rotor experimental rig. The experimental results are in accordance with the theoretical simulation results. The results are summarized as follows:

(1) The vibration displacement waveforms of rotors exhibit the "waveform cutting" characteristics.

The axis trajectory of rotors presents the obvious contraction in rubbing location. Comparing with the dynamic simulation results, the axis trajectory of outer rotor is more stable.

(2) The spectrums of vibration displacement under rubbing status not only contain the fundamental frequencies of inner and outer rotor, sometimes difference frequency and superharmonic frequency (such as $2f_L$, $2f_H$, $3f_H$, $4f_H$, and $5f_H$), but also contain combined frequencies of fundamental frequencies of inner and outer rotor, namely, $mf_H \pm nf_L$, $(m, n = 1, 2, \ldots)$. However, by comparison, it can be found that the spectrums of experimental results also contain the combined frequency components of outer rotor multiple harmonic components and inner rotor fractional harmonic components, namely, $mf_H + nf_L$, ($m = 1, 2, \ldots, n$ denotes fractional number).

(3) The single or multiple rubbing contact is conducted in rubbing experiments, which is in accordance with the dynamic simulation.

Competing Interests

There is no conflict of interests regarding the publication of the paper.

Acknowledgments

The project is supported by the National Natural Science Foundations of China (no. 11572167).

References

[1] A. Muszynska, "Rotor-to-stationary element rub-related vibration phenomena in rotating machinery—literature suryey," *Shock & Vibration Digest*, vol. 21, no. 3, pp. 3–11, 1989.

[2] S. Ahmad, "Rotor casing contact phenomenon in rotor dynamics—literature survey," *Journal of Vibration & Control*, vol. 16, no. 9, pp. 1369–1377, 2010.

[3] R. F. Beatty, "Differentiating rotor response due to radial rubbing," *Journal of Vibration & Acoustics*, vol. 107, no. 2, pp. 151–160, 1985.

[4] W.-M. Zhang, G. Meng, D. Chen, J.-B. Zhou, and J.-Y. Chen, "Nonlinear dynamics of a rub-impact micro-rotor system with scale-dependent friction model," *Journal of Sound and Vibration*, vol. 309, no. 3–5, pp. 756–777, 2008.

[5] Y. Chen and H. Zhang, "Review and prospect on the research of dynamics of complete aero-engine systems," *Acta Aeronautica et Astronautica Sinica*, vol. 32, no. 8, pp. 1371–1391, 2011.

[6] M. Torkhani, L. May, and P. Voinis, "Light, medium and heavy partial rubs during speed transients of rotating machines: numerical simulation and experimental observation," *Mechanical Systems & Signal Processing*, vol. 29, no. 29, pp. 45–66, 2012.

[7] M. A. Abuzaid, M. E. Eleshaky, and M. G. Zedan, "Effect of partial rotor-to-stator rub on shaft vibration," *Journal of Mechanical Science & Technology*, vol. 23, no. 1, pp. 170–182, 2009.

[8] Y.-S. Choi, "On the contact of partial rotor rub with experimental observations," *KSME International Journal*, vol. 15, no. 12, pp. 1630–1638, 2001.

[9] T. H. Patel, M. J. Zuo, and X. Zhao, "Nonlinear lateral-torsional coupled motion of a rotor contacting a viscoelastically suspended stator," *Nonlinear Dynamics*, vol. 69, no. 1-2, pp. 325–339, 2012.

[10] F. Chu and W. Lu, "Experimental observation of nonlinear vibrations in a rub-impact rotor system," *Journal of Sound and Vibration*, vol. 283, no. 3–5, pp. 621–643, 2005.

[11] S.-J. Wang, M.-F. Liao, Y.-F. Jiang, and X.-F. Ding, "Experimental study on local rub-impact fault of counter-rotating dual-rotor," *Journal of Propulsion Technology*, vol. 34, no. 1, pp. 31–36, 2013.

[12] W. M. Zhang and G. Meng, "Stability, bifurcation and chaos of a high-speed rub-impact rotor system in MEMS," *Sensors & Actuators A: Physical*, vol. 127, no. 1, pp. 163–178, 2006.

[13] Ahrens, J. Ulbrich, H. Ahaus et al., "Measurement of contact forces during blade rubbing," *Open Access Fund at the University of Kansas*, vol. 8, no. 12, Article ID e1003155, 2012.

[14] G. Chen, C. G. Li, and D. Y. Wang, "Nonlinear dynamic analysis and experiment verification of rotor-ball bearings-support-stator coupling system for aeroengine with rubbing coupling faults," *Journal of Engineering for Gas Turbines & Power*, vol. 132, no. 2, Article ID 022501, 2010.

[15] C. Padova, J. Barton, M. G. Dunn, and S. Manwaring, "Experimental results from controlled blade tip/shroud rubs at engine speed," *ASME Journal of Turbomachinery*, vol. 129, no. 4, pp. 713–723, 2007.

[16] B. Wang, J. Zheng, and G. Lu, "Rubbing contact between rotating blade and casing plate, part 1—experimental study," *Key Engineering Materials*, vol. 233–236, pp. 725–730, 2003.

[17] F. K. Choy and J. Padovan, "Non-linear transient analysis of rotor-casing rub events," *Journal of Sound and Vibration*, vol. 113, no. 3, pp. 529–545, 1987.

[18] C. Padova, J. Barton, M. G. Dunn et al., "Development of an experimental capability to produce controlled blade tip/shroud rubs at engine speed," *Journal of Turbomachinery*, vol. 127, no. 4, pp. 726–735, 2005.

[19] N. Bachschmid, P. Pennacchi, and A. Vania, "Thermally induced vibrations due to rub in real rotors," *Journal of Sound and Vibration*, vol. 299, no. 4-5, pp. 683–719, 2007.

[20] G. Jacquet-Richardet, M. Torkhani, P. Cartraud et al., "Rotor to stator contacts in turbomachines. Review and application," *Mechanical Systems & Signal Processing*, vol. 40, no. 2, pp. 401–420, 2013.

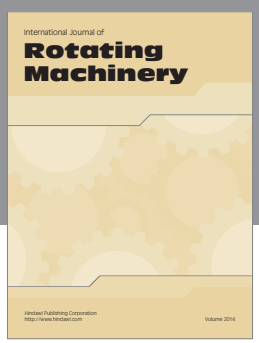

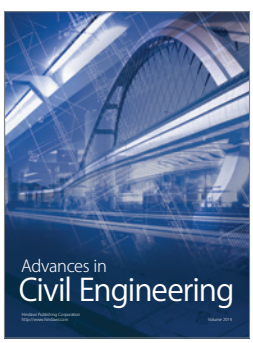

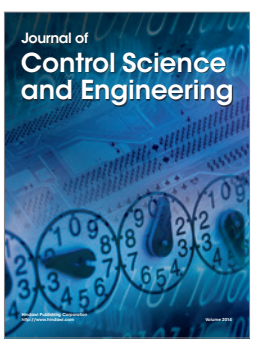

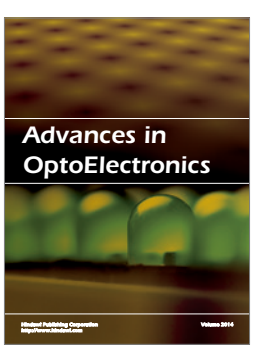

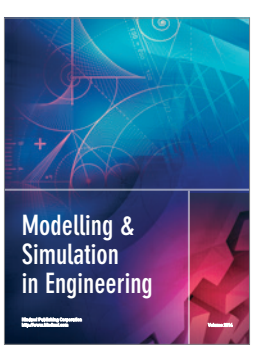

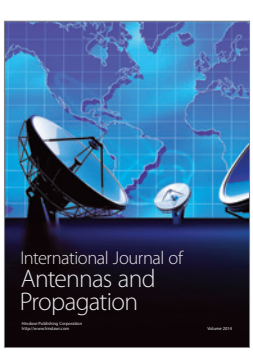

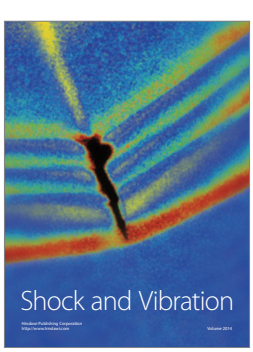

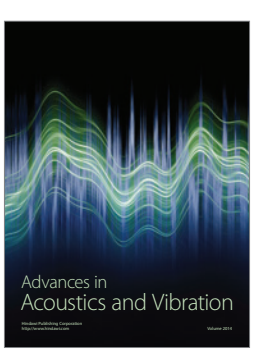

Hindawi

Submit your manuscripts at
http://www.hindawi.com